JOURNAL OF MATERIALS SCIENCE 30 (1995) 573–582

# Morphology and properties of acrylate styrene acrylonitrile/polybutylene terephthalate blends

C. M. BENSON, R. P. BURFORD
*Department of Polymer Science, University of New South Wales, Sydney, Australia 2052*

The structure and mechanical properties of acrylate styrene acrylonitrile (ASA) and ASA/polybutylene terephthalate (PBT) blends have been studied. The morphology of ASA is found to conform to a previous model. 40/60 and 60/40 blends of ASA/PBT have a two-phase, dispersed morphology while the 50/50 blend is shown to have a co-continuous structure. As processing temperature is increased, the mechanical properties decrease, due to PBT degradation. The 60/40 ASA/PBT blend has very poor impact resistance because of the continuous, degraded PBT matrix. Better mechanical properties are observed for blends with a continuous ASA matrix, particularly in the 50/50 blend. Fracture surface analysis reveals a unique morphology of mushroom-like PBT fibrils for the low processing temperature samples near the crack tip. This is thought to occur due to the competition of cohesion and adhesion of the PBT with the ASA matrix.

## 1. Introduction

Over the last twenty years, there has been a great deal of development in the area of polymer blends [1]. Under appropriate conditions, blends may have mechanical behaviour greater than that of the constituent homopolymers [2] allowing efficient recycling. One recent focus is in "rigid–rigid" polymer blends [3]; these comprise two or more thermoplastic polymers, each with a glass transition above room temperature. These blends can combine the desired properties of each of the components, such as high-temperature performance, toughness and solvent resistance.

Rigid–rigid toughening involves the addition of a second rigid phase to an already rigid matrix, to relieve triaxial tension in front of the crack tip and to generate multiple stress concentration sites around the crack tip [4]. It was the aim of the present work to combine two rigid polymers suitable for demanding engineering applications.

Factors which affect the toughness of polymeric materials include the presence of rubber particle inclusions [5, 6], ability to craze [6], shear banding and debonding or cavitation [7], interfacial adhesion [8], interphase adhesion and anisotropy [9]. These factors are all affected by processing conditions and their effect may be studied by mechanical testing and electron microscopy of suitably processed samples.

The majority of the above factors are affected by the brittle–tough transition. Homo-polymers and polymer blends exhibit brittle or ductile behaviour depending on intrinsic morphology and chain structure, as well as the extrinsic properties of temperature, rate of strain and specimen geometry. The brittle–ductile transition behaviour holds for largely amorphous polymers and will be justified later. Wu [10] has described two chain parameters, entanglement density and the characteristic ratio, unique to each polymer, that can be manipulated to shift the brittle–ductile transition. These are essentially the number of chain junctions per unit volume and a function of chain end-to-end distance, respectively, and may be readily calculated for each matrix polymer.

Wu [10] has defined three classes of blends based on matrix type. His studies indicate that intrinsic toughness is controlled by the chain parameters of the matrix polymer. In theory, the matrix phase also determines the morphology of the dispersed phase. The brittle matrix deforms and fractures mainly by crazing, but adding rubber particles the toughness can be increased. This is maximized with a matrix entanglement density of $\sim 0.1$ mmol $cm^{-3}$ (for example, styrene acrylonitrile copolymer, SAN) where both yielding and crazing are found to occur. Further toughening is also possible by optimizing particle size, which Wu also found to be dependent on entanglement density.

The failure mode in a ductile matrix is largely yielding and the rubber particles need to conform to a critical size range to toughen these matrices. The critical particle size is dependent on the rubber volume fraction and interparticle distance. The critical interparticle distance, $T$, is dependent on the characteristic ratio of the matrix (for example in polyethylene terephthalate, PET). This is known as the "percolation" theory of toughening. The rubber particles cavitate and debond themselves from the matrix, absorbing energy and relieving stress in front of the crack tip and forming thin ligaments of matrix between the voids of rubber. If the rubber particles are close enough together (less than the $T$) the stress is distributed over a large area due to the rubber particle/matrix forming a pervasive network, relieving the

0022–2461  

stress at the crack tip and allowing yielding to occur. The matrix ligaments also yield and hence toughen the polymer. This theory is similar to that developed by Sue [4] who describes craze-void ("CROID") behaviour. The third type of behaviour is a combination of the above two and little is known of the precise mechanisms of deformation.

Acrylate styrene acrylonitrile (ASA) is a rubber–toughened SAN. It has already been shown [11, 12] to have enhanced toughness by fracturing after crazing and yielding. Like high impact polystyrene (HIPS) it is a two-phase material, comprising an SAN matrix with acrylate rubber particles dispersed with SAN inclusions. It has similar properties to acrylonitrile butadiene styrene terpolymer (ABS), with the added advantage of enhanced weatherability. There has been very little published research on ASA, despite it having potential as a rigid–rigid toughened material.

A system of ASA, containing up to 42 wt % rubber, can be considered as a two-phase co-continuous structure, such as a thermoplastic interpenetrating polymer network (IPN) [13], if the rubber phase is in a continuous form. If so, one might see some synergistic characteristics, with the blend properties exceeding those predicted by the weighted average of the constituent polymers. However, as seen later, the rubber-rich component, whilst aggregating into rubber-rich phases, is by no means microscopically homogeneous but comprises of groups of smaller rubber particles. Therefore, it is appropriate to combine theories of Wu and others, of toughened plastics containing small ($< 1$ μm) discrete particles with the structural model proposed by Munstedt [11] for ASA (Fig. 1).

Munstedt describes ASA as being made up of small individual particles of rubber with grafted SAN in an SAN matrix. The rubber particles conglomerate into what appears to be cell-like structures, with the contained matrix immobilized as long as the cell structure is intact. When the material is taken to the yield stess, the cell structure breaks down. The rubber particles are dispersed and the matrix deformed. Where the concentration of rubber domains is high and dispersion is reasonably uniform, a semicontinuous network of toughened material exists. This allows substantial bulk extension (i.e. strain) until, at some stage, the network collapses. As strain further increases, particles are separated by distances greater than the critical interparticle distance, $T$, and no toughening is imparted. Failure then occurs by matrix yielding.

In the case of ASA alone, as reported by Munstedt, the concentration of rubber can either be high (42 wt %) or low (18 wt %). The microstructure given in Fig. 1, departs from the simple binary rubber particle/plastic matrix model used by Wu [10], but the rubber particles are shown to similarly aggregate as a network. At low rubber concentrations there are rubber-rich regions, tied together with narrower strings of rubber particles. After straining, Munstedt showed by TEM that the rubber becomes nearly uniformly dispersed with the aggregates breaking down. The interparticle distance would seem to be about 0.05–0.15 μm which is higher than the $T$ for SAN of $\sim 0.05$ μm [10].

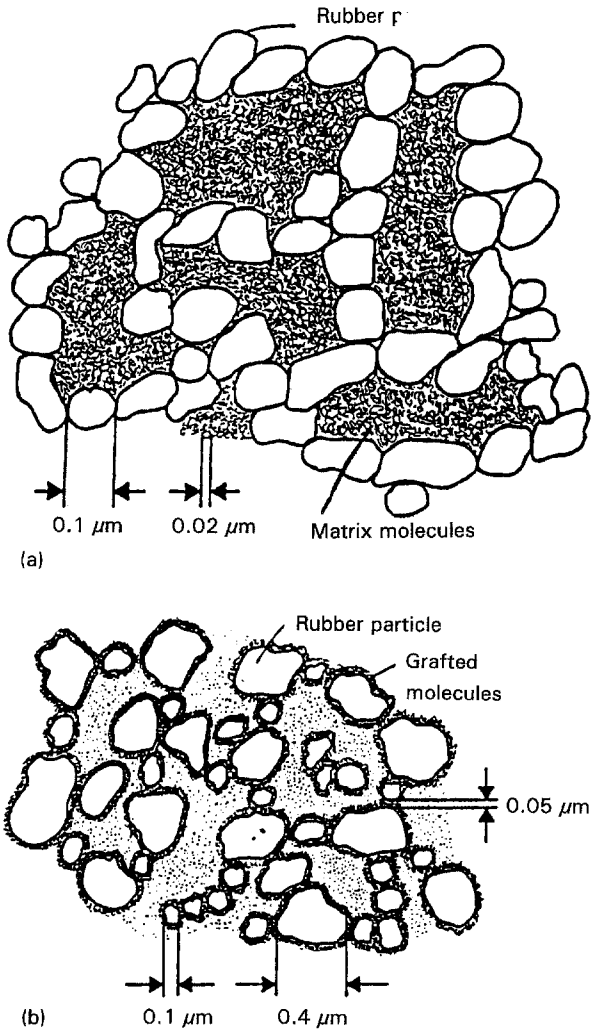


*Figure 1* (a) Munstedt's model of ASA showing the rubber particle cell structure. (b) ASA model showing the initial break down of the cell structure.

It is important to note, that the ASA used in the present study contains 42 wt % rubber, which is higher than that of the stressed ASA shown by Munstedt, and so both Munstedt's model and the percolation theory are predicted to apply. However, the primary emphasis is directed towards ASA/polybutylene terephthalate (PBT) blends, for which we believe very little previous information has been published.

Several blends based on ABS have been established commercially, including ABS polycarbonate (PC), Terblend B (BASF) and Bayblend (Bayer-Mobay) and ABS/Polyamide, Ultramid-Terluran (BASF) and Triax 1000 (Monsanto). One might a priori consider them comparable with ASA/polyester blends, although despite their chemical similarities, important differences exist [14]. However, the micromechanisms of these are not well established and important structural and processing difficulties exist. For example the rubber component of ASA is far more thermally stable than the polybutadiene in ABS. This is significant as particularly high processing temperatures are required for PET. In addition, PBT can be processed at lower temperatures than PET and crystallization kinetics and other attributes differ for the two polymers.

Both polybutylene terephthalate (PBT) and polyethylene terephthalate (PET) are pseudoductile materials. They are able to be toughened by rubber inclusions and fit the rigid criteria. All three polymers contain sufficient amorphous material to follow the theories of Wu and Sue. In this work the mechanical and morphological results have been compared to determine if these materials do fit this criterion.

## 2. Experimental procedure

### 2.1. Materials

The samples used in this study were prepared from commercial grades of ASA (Luran S) and PBT (Ultradur) supplied by BASF, Melbourne. The two materials were mixed in a volume ratio of 60:40, 50:50 and 40:60 of ASA to PBT, as these were recommended by BASF to closely approximate some of their commercial blends. The mixed blends were processed by either extrusion or injection moulding.

#### *2.1.1. Extrusion*

The mixed pellets were processed by a single pass in a Haake Rheocord Systems 90 twin screw extruder. The extruded strip, 30 mm × 3 mm in cross-section, was water quenched and aged at 25 °C for several days before tensile bars were punched in accordance with ASTM D 638, type C. The strip was formed by processing at temperatures ranging from 230–280 °C at 10 °C intervals, the four temperature zones being ramped by 10 °C each. The feed zone was therefore 30 °C lower than the die, with the latter temperature being designated as the processing temperature. Typical screw speeds ranged from 20–30 r.p.m., corresponding to shear rates of 4–8 $s^{-1}$ and residence times of 2–3 min.

#### *2.1.2. Injection moulding*

The mixed pellets were processed by a single pass through a Boy 15S injection moulding machine. A two-cavity mould, consisting of a standard tensile bar and Charpy impact bar (unnotched), was employed using a conventional runner-gate path. The specimens were processed at temperatures ranging from 230–280 °C at 10 °C intervals, with the two temperature zones ramped by 10 °C. Again, the die temperature is used to indicate the temperature of processing. Cooling water was fed at 20 °C to the mould. Temperature control and uniformity was not as accurately achieved as for the extruded samples.

Impact bars were notched in accordance with ASTM D 256 using a standard fly cutter and broken using a conventional pendulum apparatus, with at least ten repetitions per data point. All tensile bars were tested on an Instron TT-AL universal machine modified with a digital follower/control unit. The crosshead speed was 5 mm $min^{-1}$ and at least five replicates for each material were determined. Errors ranged from 15%–25 % for tensile tests (increasing with temperature) and 10%–25 % for impact tests (decreasing as temperature increases).

### 2.2. Microscopy

Sample morphology was studied using a Hitachi 7000 TEM, operating at an accelerating voltage of 75 kV. Samples were prepared by taking sections of the extrudate and injection-moulded specimens both parallel and perpendicular to the direction of extensional force. The samples were glued to a stub and trimmed with a fresh razor blade to around 1 mm square. The samples were then stained with ruthenium solution as described by Montezinos *et al.* [15] for at least 16 h. The samples were then further trimmed using a fresh glass knife on a Riechet-Jung ultramicrotome, to around 0.1 mm square. Thin sections were then cut using a diamond knife on the same ultramicrotome.

Fracture surfaces were studied using both a Cambridge 360 SEM and a Hitachi FESEM. Samples were prepared by staining with ruthenium for at least 16 h. The SEM samples were then sputter coated with gold/palladium. The FESEM samples were coated with chromium.

## 3. Results and discussion

### 3.1. Mechanical behaviour

Tables I and II and Figs 2 and 3 show the tensile strength and impact resistance of ASA and PBT blends, after processing at temperatures of 230–280 °C, to determine a suitable set of operating conditions. A slight increase in tensile strength occurs as the temperature is increased, but elongation at break is less than that of the lower temperature samples. At the highest temperatures, substantial embrittlement occurs, reflected also by low impact values.

For the 40:60 ASA:PBT blend, impact resistance decreases markedly as temperature increases. This is because the PBT matrix degrades rapidly at temperatures $\geqslant$ 270 °C, as confirmed by Fourier transform–infrared microscopy (FT–IR). The absorbance peak of the OH group is larger for the samples processed at higher temperatures, after spectra are normalized using the carbonyl peak. This indicates that the ester linkage is degraded into the OH groups as temperature is increased. The other two ASA-rich blends are not as strongly affected as they both have a continuous ASA matrix, and so have better impact strength than the PBT-rich blend. For a combination of tensile strength and impact resistance, the 50:50 blend of ASA and PBT is best, particularly after processing at lower temperatures.

The 50:50 and 60:40 blends have improved tensile strengths compared with ASA alone, but maintain the desirable impact properties of the ASA. Blends may therefore be employed in a wider range of applications than ASA alone.

### 3.2. Morphology

#### *3.2.1. ASA*

The morphology of ASA has been infrequently reported in the literature [11, 15, 16] with the only detailed account by Munstedt [11]. The morphology

TABLE I Tensile properties of ASA/PBT blends

| | Temperature (°C) | Stress, $F/A$ | Strain (%) | Modulus, $E$ |
|---|---|---|---|---|
| ASA extruded | 240 | 20.7 | 22.0 | 100 |
| | 250 | 19.8 | 19.7 | 100 |
| | 260 | 18.9 | 20.5 | 100 |
| | 270 | 17.7 | 18.6 | 100 |
| | 280 | 13.3 | 8.5 | 150 |
| ASA/PBT, 50/50 blend extruded | 230 | 28.4 | 12.8 | 220 |
| | 240 | 25.7 | 8.3 | 300 |
| | 250 | 18.0 | 4.5 | 450 |
| | 260 | 13.0 | 2.6 | 500 |
| | 270 | 13.4 | 2.2 | 630 |
| ASA/PBT, 60/40 blend extruded | 230 | 25.5 | 11.5 | 200 |
| | 240 | 25.9 | 10.7 | 250 |
| | 250 | 23.3 | 8.2 | 300 |
| | 260 | 24.9 | 8.5 | 300 |
| | 270 | 13.0 | 2.5 | 500 |
| ASA/PBT 50/50 blend | 230 | 28.6 | 4.8 | 600 |
| | 240 | 28.0 | 5.1 | 550 |
| | 250 | 24.5 | 3.8 | 650 |
| | 260 | 16.2 | 2.2 | 750 |
| | 270 | 13.0 | 1.7 | 750 |
| ASA/PBT 60/40 blend | 230 | 30.0 | 5.2 | 600 |
| | 240 | 26.5 | 4.3 | 650 |
| | 250 | 23.0 | 3.5 | 650 |
| | 260 | 20.2 | 2.9 | 700 |
| | 270 | 11.6 | 1.3 | 900 |
| ASA/PBT 40/60 blend | 230 | 27.0 | 4.1 | 650 |
| | 240 | 22.0 | 3.2 | 700 |
| | 250 | 15.5 | 2.2 | 700 |
| | 260 | 8.2 | 1.1 | 750 |
| | 270 | 7.3 | 0.9 | 850 |

TABLE II Charpy impact data of ASA/PBT blends

| Temperature (°C) | Charpy impact strength ($Jm^{-1}$) | | |
|---|---|---|---|
| | 60/40 | 50/50 | 40/60 |
| 230 | 30 | 30 | 30 |
| 240 | 25 | 25 | 20 |
| 250 | 20 | 20 | 15 |
| 260 | 20 | 20 | 10 |
| 270 | 20 | 20 | 10 |

and micromechanics of ASA and PBT blends have not, to our knowledge, been previously revealed.

The ASA used in this study contains 42 wt % rubber and is comparable to one of the types used by Munstedt. The morphology obtained for our ASA, shown in Fig. 4a and b, corresponds very closely to that shown previously. This close agreement for the single ASA component serves to legitimize the morphology given for the subsequent, more complex and

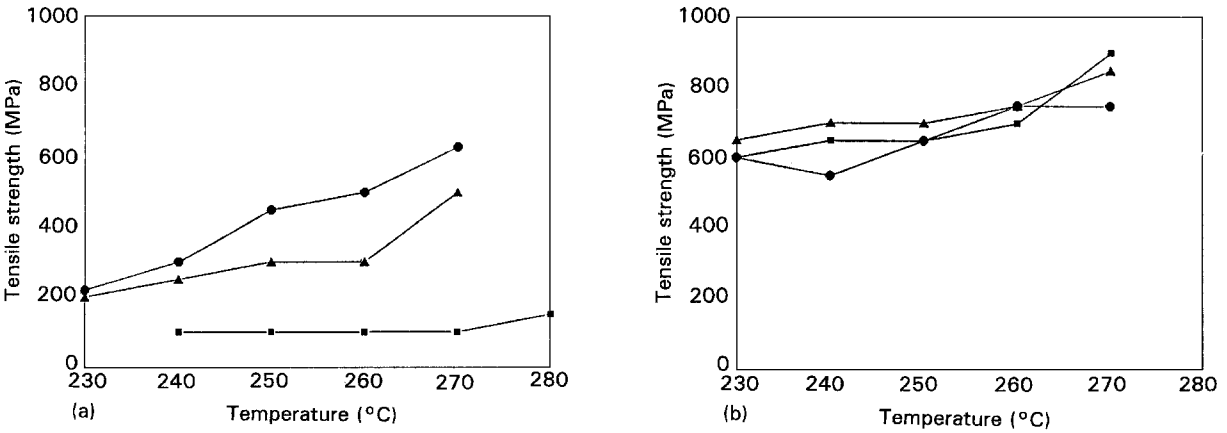


*Figure 2* Tensile strength at break against processing temperature of the ASA/PBT blends: (a) extruded blends, and (b) injection-moulded blends. (a) (▲) 60:40, (●) 50:50, (■) 100:0; (b) (■) 60:40, (▲) 40:60, (●) 50:50.

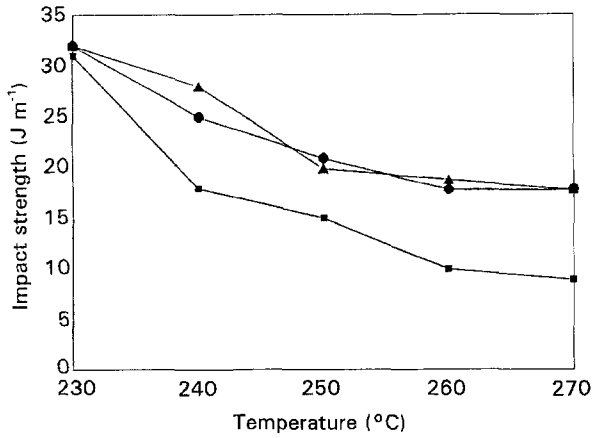


*Figure 3* Impact resistance versus processing temperature of the ASA/PBT blends: (■) 40:60, (▲) 50:50, (●) 60:40.

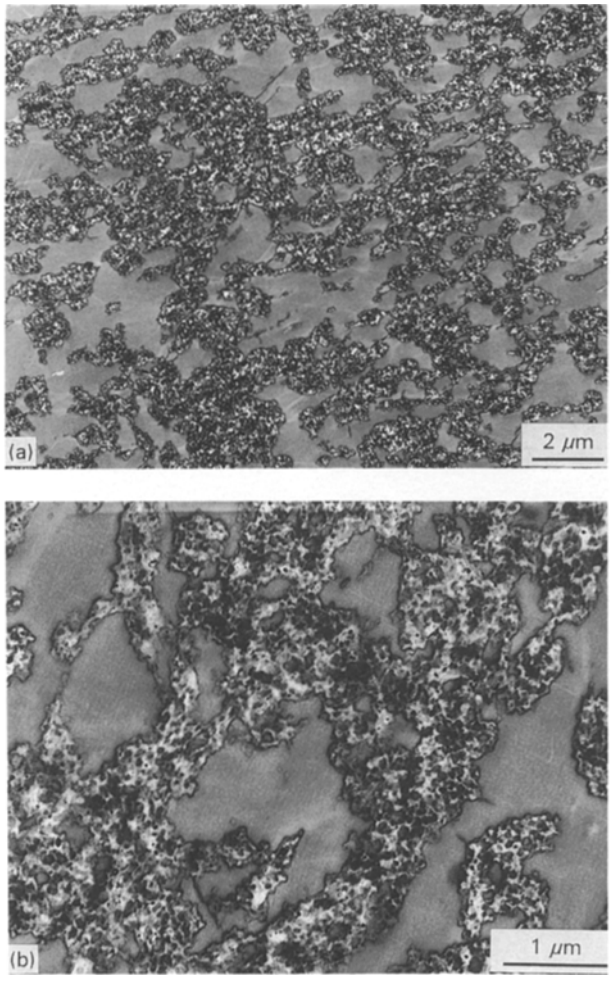


*Figure 4* (a, b) Transmission electron micrograph of ASA stained with ruthenium. Note the rubber particle cell structure in (b).

previously unreported blends, as sample and preparation conditions were kept constant. The morphologies we find conform well with Fig. 1, but some large groupings of rubber particles with areas of matrix inclusions, similar to that described by Ban *et al.* [17], can also be found, as shown in Fig. 4b. The size of the inclusions varies from very small, $< 0.1$ μm, through medium, 0.2 μm, to large, $> 0.5$ μm. Some minor fragmented areas can also be observed, conforming to Munstedt's model.

### 3.2.2. ASA:PBT blends

The blends of ASA and PBT shown in Figs 5–7 depict two well-defined phases, the PBT being continuous and dark. In the 40:60 ASA:PBT blend, the ASA is formed as pockets within the continuous PBT matrix. Significantly, the rubber particles do not migrate into the PBT phase or to the interface of the two phases, but rather stay within the SAN matrix, causing no visible change [18]. Similarly, in the 60:40 blend, the ASA is the dominant phase and the PBT is dispersed throughout the ASA matrix. Again, the rubber particles stay in the SAN matrix.

The 50:50 blend, however, appears as a co-continuous matrix (Fig. 7). This blend reflects maximum compatibility between the constituents and has the best combination of tensile strength and impact resistance. The extrudate in this case was more coherent, with greater firmness compared to the relative weak consistency of the 40:60 blend where the low viscosity of the PBT phase at the operating temperatures produced a poor-quality extrudate.

One explanation for the improved performance of the blends over the ASA and PBT single matrices can

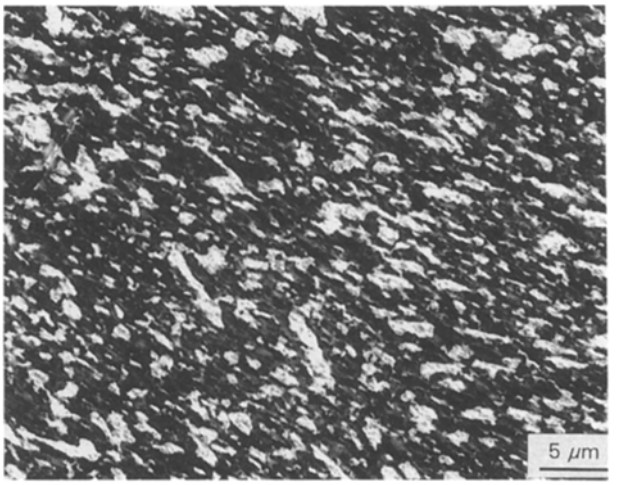


*Figure 5* Transmission electron micrograph of 40/60 ASA/PBT blend showing the dispersed ASA phase. The continuous dark phase is PBT.

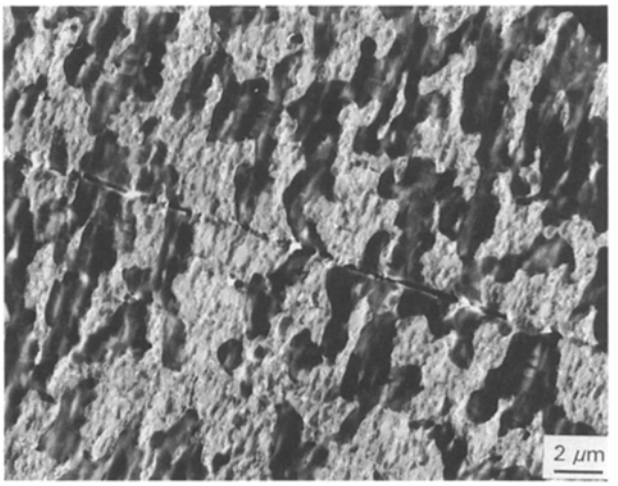


*Figure 6* Transmission electron micrograph of 60/40 ASA/PBT blend showing continuous ASA matrix.

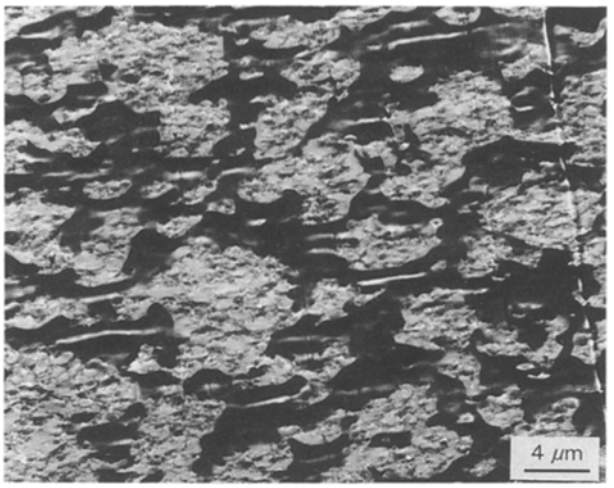


*Figure 7* Transmission electron micrograph of the 50/50 ASA/PBT blend showing a co-continuous structure.

be found by adapting the Munstedt model. As the ASA approaches the yield stress, the cell structure of the rubber particles is broken down, with inter-particle distance being too great to allow percolation [10] or bridging between adjacent particles. For blends however, the ASA domains are small, being typically $< 5$ μm. This and the high concentration of rubber means that a greater yield stress needs to be applied to separate the rubber particles sufficiently to prevent percolation and bridging. This is similar to that found by Kim *et al.* [19] for ABS materials, where the increase in rubber particle dispersion was found to cause decreases in mechanical strength. However, the mechanical properties of ternary phase blends can depend on many factors, including morphology [18], making unambiguous conclusions difficult.

The improved performance of the blends over the constituent homopolymers could suggest that further means of bonding the two phases, such as compatibilizers or glass fibres, could lead to much greater improvements in mechanical strength.

## 3.3. Orientation

It has long been known that processing can cause orientation of filled materials in the direction of the extensional force and large areas of orientation can cause a decrease in strength in the direction perpendicular to orientation [9]. Here we determine whether orientation occurs under our processing conditions, because this may affect the fracture mechanics data. The three-dimensional TEM analysis used to demonstrate any orientation also enables a more rigorous interpretation of structure–property relationships. Both extruded and injection-moulded samples were examined for any process-induced orientation.

To ensure that the morphology seen is, in fact, due to processing, a detailed sectioning procedure was conducted, as outlined in Section 2.2. If the sectioning process itself was to cause any orientation artefact, then the same orientation would be seen in both the parallel and perpendicular directions. Figs 4–7, taken in the $x$–$y$ plane, show that there is, in fact, little or no orientation, possibly occurring only at the lowest processing temperature. This might be predicted on the basis of higher sample viscosities and so greater deformation at the higher forces applied.

## 3.4. Fracture surfaces

Examination of the fracture surface reveals a number of features. Firstly, mushroom-like shapes occur in the area near the crack tip of the low-temperature samples, Fig. 8a, b, whilst after higher temperature processing, fibril like shapes appear instead (Fig. 8c).

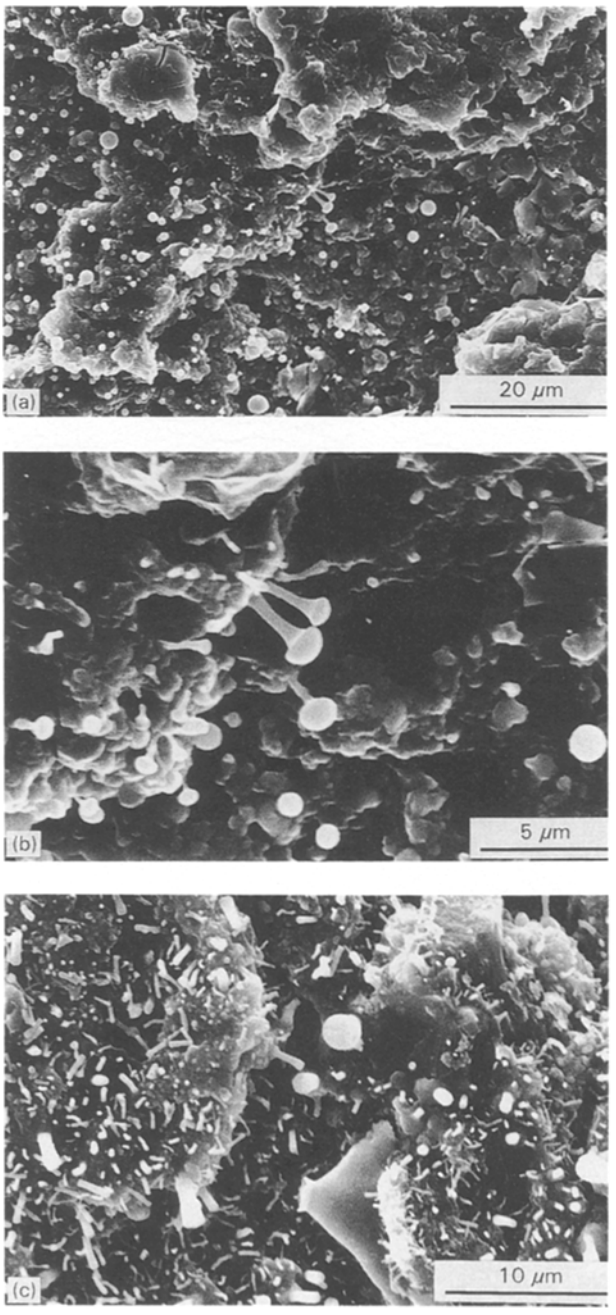


*Figure 8* (a, b) Scanning electron micrograph of the fracture surface (fast fracture region) of a 50/50 ASA/PBT blend with a processing temperature of 230 °C. Note their frequency (a) and the mushroom-like rubber fibrils (b) appearing white due to staining (c) Scanning electron micrograph of the fracture surface (fast fracture region) of a 50/50 ASA/PBT blend with a processing temperature of 270 °C. The rubber fibrils are white due to staining, but there are no mushroom-shaped fibrils.

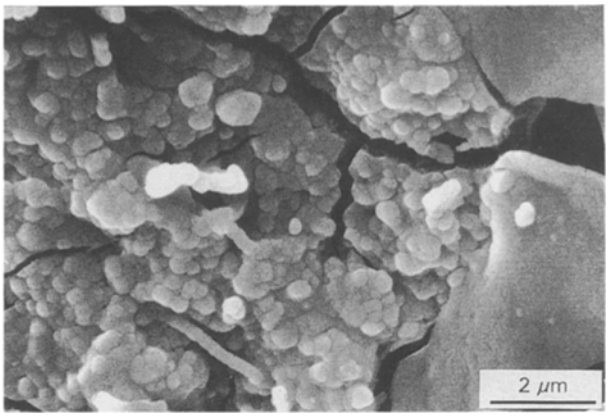


*Figure 9* Scanning electron micrograph of a fracture surface away from the crack tip. There is no fibrillation of the rubber. Cracks can be seen to grow around the rubber particles, indicative of debonding.

Mushrooms are typically 2–4 μm long, with shaft widths of about 0.5 μm and heads around 1–2 μm diameter. It is conceivable that these mushrooms and fibrils are either PBT or the rubber fraction of the ASA, because they appear white, indicating staining. Away from the crack tip (Fig. 9) the PBT phase appears continuous and smooth, consistent with TEM observations. The ASA appears rough or bubbly due to rubber particles on the surface. It is difficult to identify from conventional scanning electron micrographs which phase generates the mushroom morphology, but FESEM is useful, as outlined below.

The higher resolution of the FESEM facilitates the identification of the phases and hence the phase from which the mushrooms form. The FESEM micrographs show that two types of mushrooms exist. The first are those in Fig. 10a–d, from the same area as those shown in the scanning electron micrographs, Fig. 8a–c, and shown to be in the PBT phase (the smoother of the two phases). The second type are more like droplets, which are also formed out of the dispersed PBT phase (Fig. 11a–d). Strong evidence of the droplets forming in the PBT phase rather than the rubber of the ASA phase is provided by Fig. 11d. This depicts a droplet that has been split through the centre. If the droplet was the rubber phase, then it would have appeared rough due to tearing at this high magnification (30 000 times). Indeed, we would expect it to cavitate or to debond from the matrix. Clearly this has not occurred and the only conclusion is that the mushrooms and droplets are formed in the PBT phase. This is further confirmed by the ASA morphology, Fig. 12, which has no mushrooms or droplets visible.

It is proposed that the droplet morphology has been developed during processing in the melt phase of the injection-moulding machine [20, 21]. The theory of morphology development of a Newtonian liquid dispersed phase in a Newtonian matrix due to extensional forces has been extensively studied [22, 23] and an attempt to adapt this to polymer blends has been made by Utracki and Shi [20]. The dispersed phase is initially spherical due to the difference in interfacial tension. As the extensional forces are increased to overcome the interfacial force, the droplets deform and break up into smaller droplets. This process is shown schematically in Fig. 13, and leads to a very similar morphology to that shown in Fig. 11.

A suggested explanation for the mechanism of the observed mushroom morphology is given in Fig. 14. The mushrooms are seen as droplets which have drawn out prior to fracture. Competition between

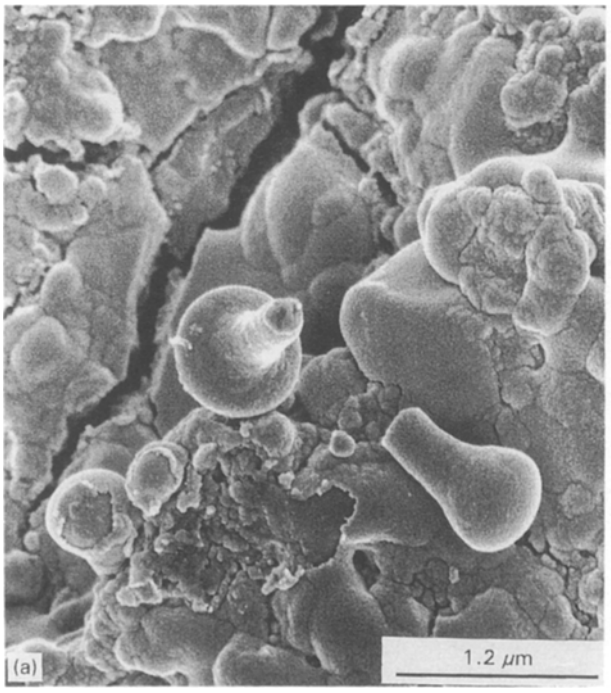


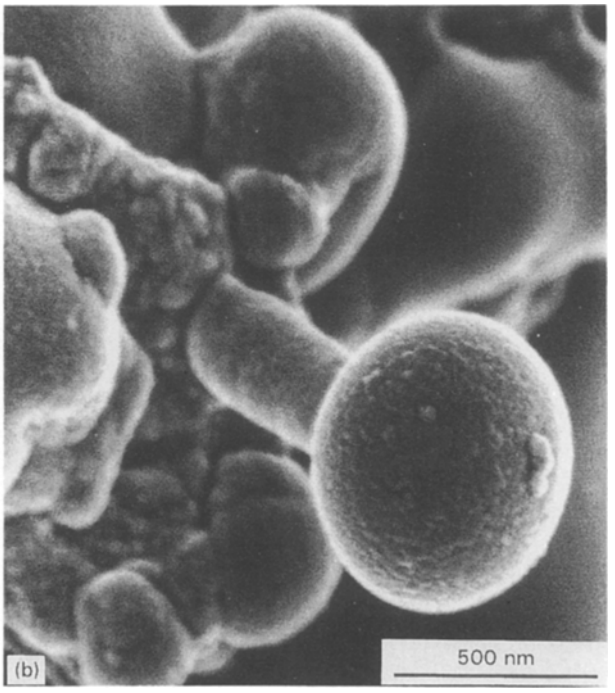


*Figure 10* FESEM of the fracture surface of a 50/50, ASA/PBT blend showing the mushroom morphology. (a) A mushroom which has broken in the stem; (b) the stems of the mushrooms are clearly drawn out; (c) the central mushroom shows extensive drawing; (d) broken stems leave a fibril morphology.

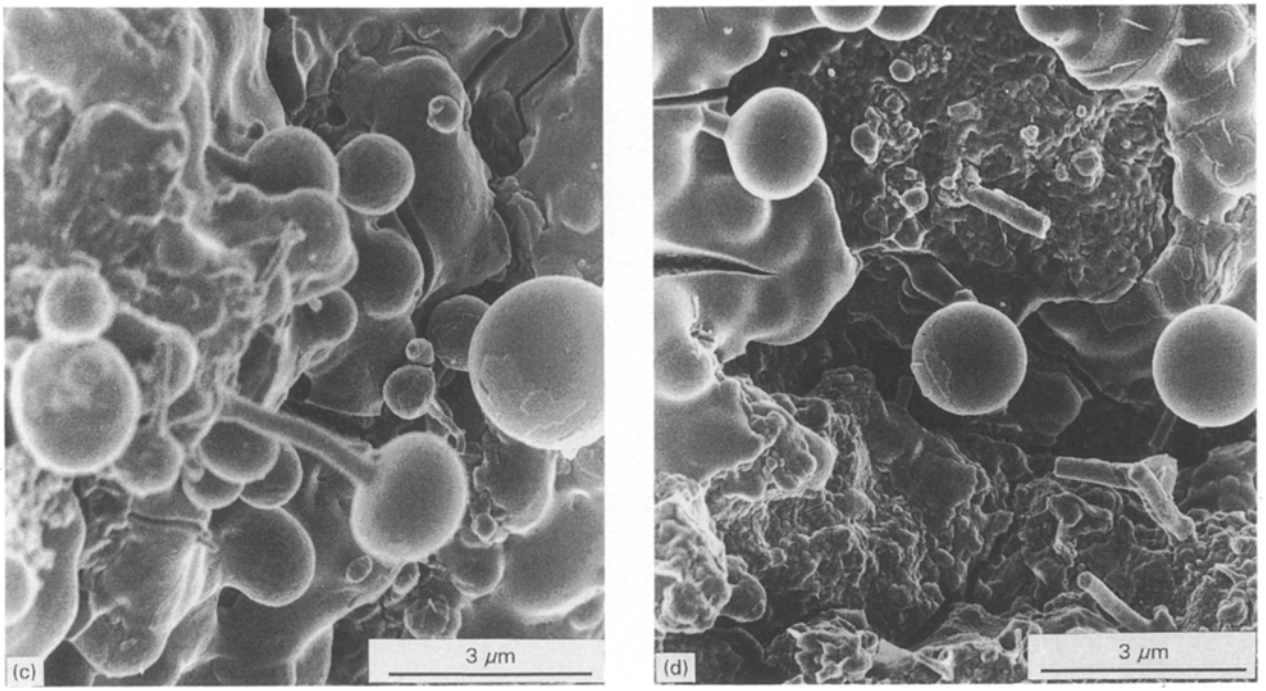


*Figure 10* (continued).

adhesion and cohesion of the PBT exists. The lower temperature samples have better cohesion, and hence when stretched, neck (to give the stem of the mushroom). When the stress exceeds the adhesion strength, the PBT droplet is detached. The shape is unchanged after fracture, as debonding occurs after necking, and the previously attached part of the PBT to the ASA matrix is not deformed. The higher temperature samples have better adhesion than cohesion, with the cohesive strength being diminished by the high temperatures experienced during processing. Whether this is due to the actual temperature used or from localized hot spots is yet to be determined. In this case, the adhesive strength is greater than cohesive strength. When the material was fractured, the PBT is less drawn out and breaks in the stem formed, leaving fibrils behind. This is reflected by these fibrils being shorter than the "mushroom" shapes observed in the low-temperature samples. As can be seen from the mechanical data, despite this morphological

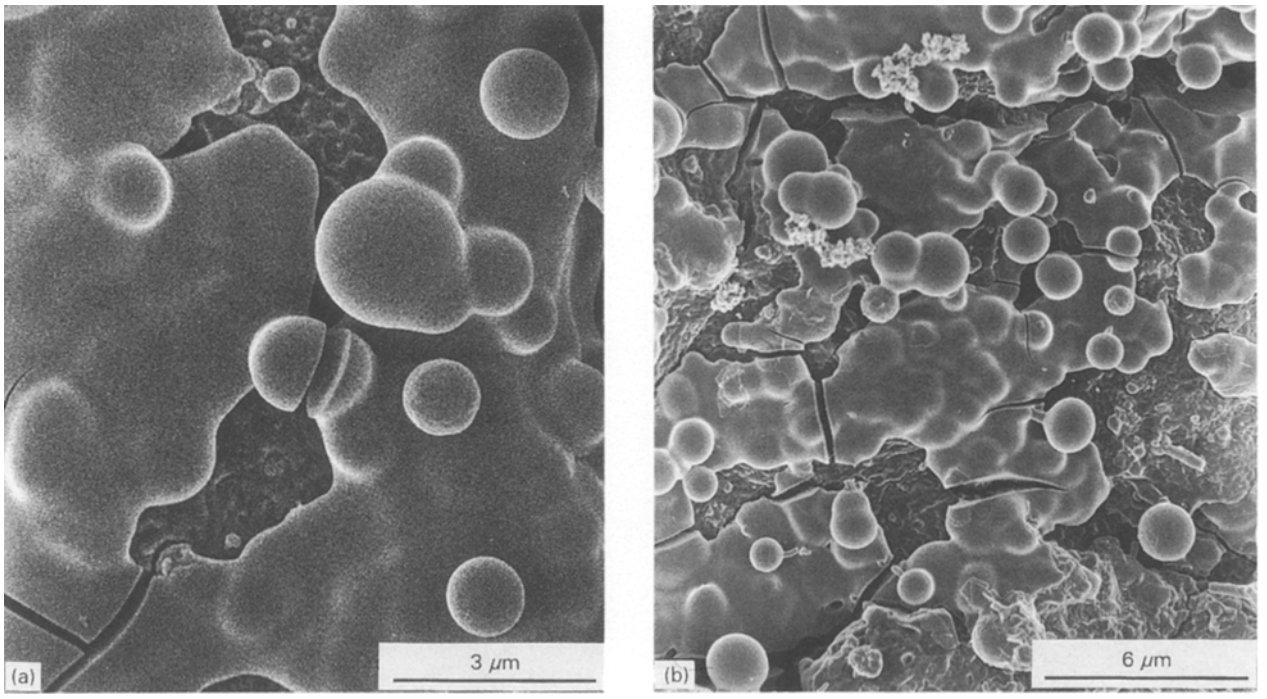


*Figure 11* FESEM of the fracture surface of a 50/50 ASA/PBT blend with droplet morphology. (a) Development of droplets from the PBT phase; (b) droplets only appear in the smoother PBT phase; (c) a droplet split through the centre; (d) higher magnification of (c) showing a clean break.

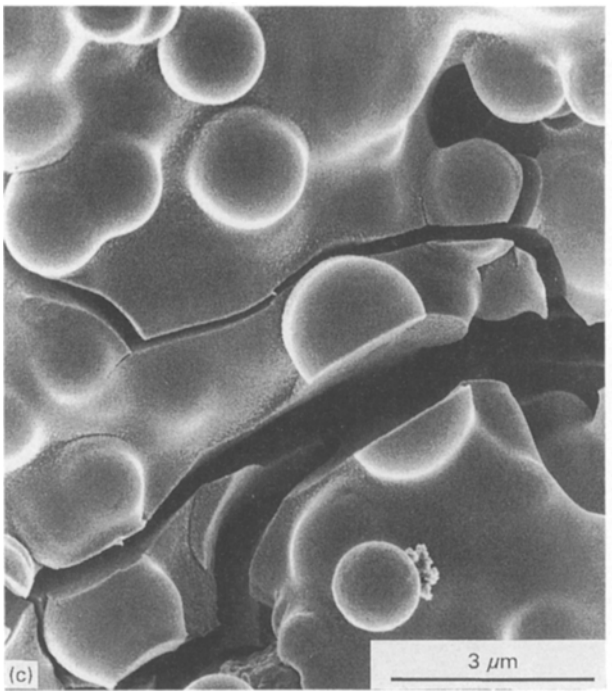


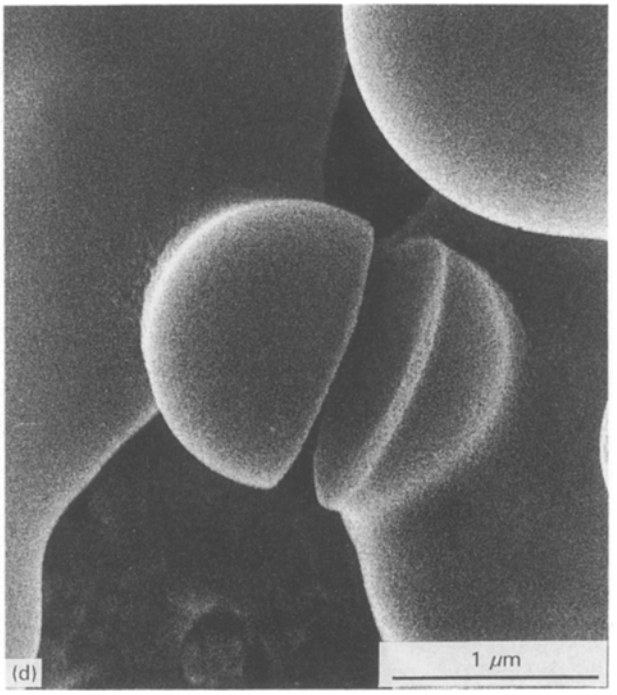


*Figure 11* (continued).

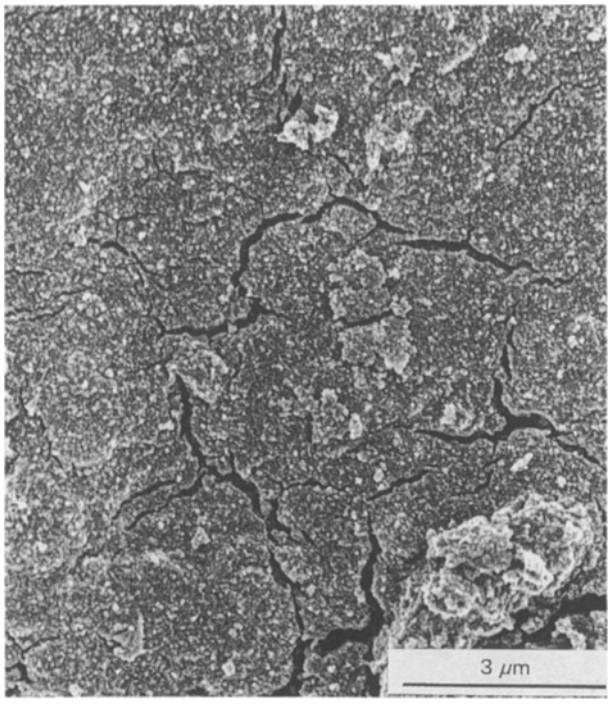


*Figure 12* FESEM of a 50/50 blend of ASA/PBT showing a region of ASA with no mushrooming.

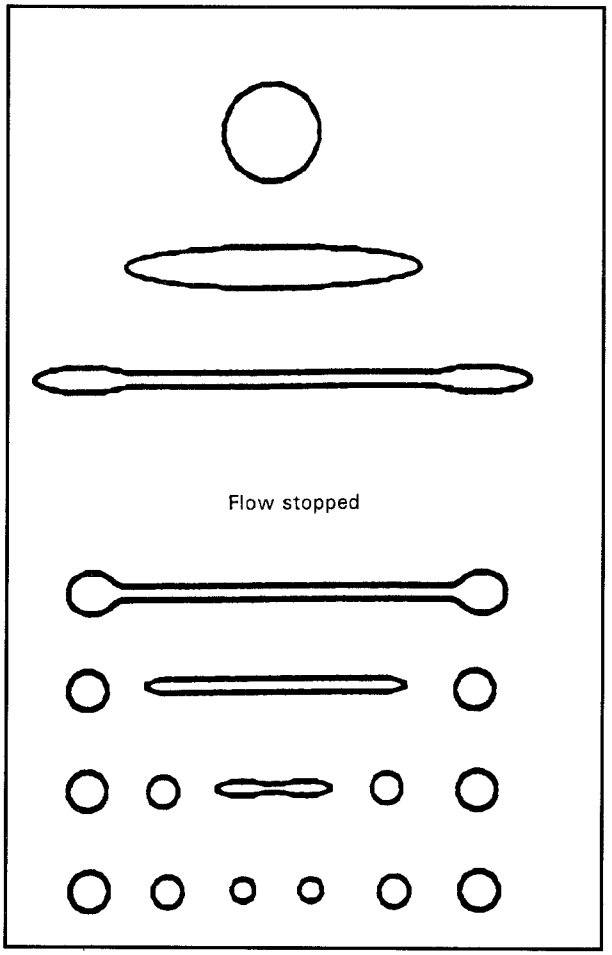


*Figure 13* Schematic diagram of droplet formation produced during processing. As processing time increases (down the diagram) the droplets break down into smaller droplets.

difference, there is no change in tensile strength. This is similar to results shown by Borggreve *et al.* [24] in the nylon–rubber system, where adhesion does not affect yield stress.

Upon further examination of the fracture surface away from the crack tip, numerous areas of microcracking are observed, with cracks in the ASA phase growing around the rubber particles (Fig. 9). This indicates that a debonding mechanism is occurring [25]. The rubber particles cause crack deviation and bifurcation, leading to multiple cracking over a large area. This process absorbs energy and toughens the material and may explain why the low-temperature samples have almost twice the impact resistance to the high-temperature samples.

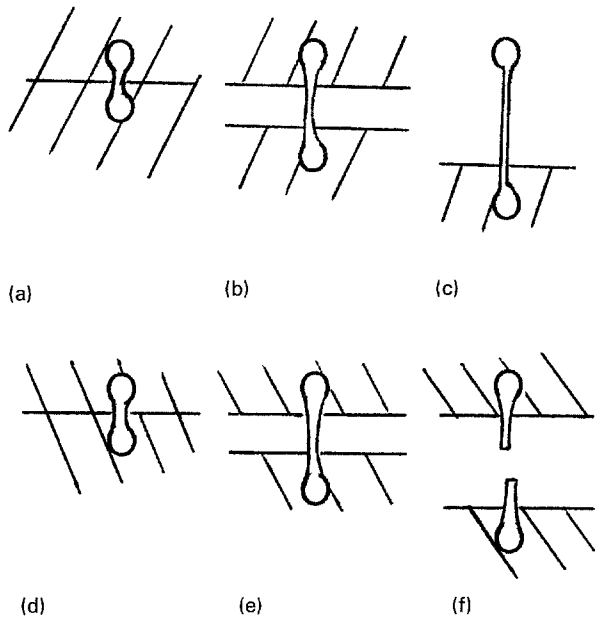


*Figure 14* The competition between cohesion and adhesion causes the mushroom-like morphology. Above, the cohesion is greater causing the PBT to stay together, as the matrix fractures, and form the mushroom shape (a–c). Below, the cohesion is diminished causing greater adhesive strength and the PBT breaks in the stem, leaving straight fibrils (d–f).

## 4. Conclusion

Processing temperature has a significant effect upon breaking strain, modulus and impact strength of ASA/PBT blends. This is largely due to the degradation of PBT at elevated temperatures. The PBT matrix is weakened as the temperature is increased, increasing the lower blend performance as the PBT content is increased. The 50:50 blend has the best tensile strength and impact resistance, due to the co-continuity of the ASA and PBT matrices. The 40:60 and 60:40 blends exhibit a two-phase, dispersed morphology.

Negligible orientation is seen in these blends by either TEM or SEM, suggesting blends have good mechanical properties when triaxial forces are applied. Fracture surfaces show a new type of morphology near the crack tip. The appearance of PBT "mushrooms" or fibrils is thought to be due to the competition of adhesion and cohesion of PBT to the ASA matrix.

## Acknowledgements

The authors thank BASF Australia for their generous supply of materials and technical advice. They also acknowledge Mr E. Kosier, RMIT Melbourne, for discussions relating to fracture surfaces, and Mr P. Marks, UNSW, for assistance with electron microscopy. This work has been supported by an Australian Research Council Grant.

## References

1. L. A. UTRACKI, "Polymer Alloys and Blends" (Hanser, New York, 1989).
2. A. K. KULSHRESHTHA, *Polym.-Plast. Technol. Eng.* **32** (1993) 551.
3. A. F. YEE and H. J. SUE, "Toughening mechanisms in alloys of rigid polymers" (The Society of Plastics Engineering, Chicago, Ill, 1987).
4. H. J. SUE, *J. Mater. Sci.* **27** (1992) 3098.
5. J. SULTAN and F. McGARRY, *Polym. Eng. Sci.* **13** (1973) 19.
6. C. B. BUCKNALL, "Toughened Plastics" (Applied Science, London, 1977).
7. A. F. YEE and R. A. PEARSON, *J. Mater. Sci.* **21** (1986) 2462.
8. H. J. SUE, H. JUANG and A. F. YEE, *Polymer* **33** (1992) 4868.
9. L. A. UTRACKI, "Progress in Polymer Processing", seminar presented at RMIT, Melbourne, 1 February 1993.
10. S. WU, *Poly. Int.* **29** (1992) 229.
11. H. MUNSTEDT, *Polym. Eng. Sci.* **21** (1981) 259.
12. K. BRIGGS, BASF Melbourne, private communication (1993).
13. W. P. GREGEN, R. G. LUTZ and S. DAVISON, "Thermoplastic Elastomers: a comprehensive review", edited by N. R. Legge (Hanser Verlag, Munich, 1987) p. 507.
14. M. A. KIRSCH and D. J. WILLIAMS, *CHEMTECH.* **24** (1994) 40.
15. D. MONTEZINOS, B. G. WELLS and J. L. BURNS, *J. Polym. Sci. Polym. Lett. Ed.* **23** (1985) 43.
16. C. K. RIEW (ed.), "Rubber Toughened Plastics", Advances in Chemistry, Series 222 (ACS, Washington DC, 1989) Ch. 2.
17. L. L. BAN, M. J. DOYLE and G. R. SMITH, *Polym. Commun.* **29** (1988) 163.
18. T. W. CHENG, H. KESKKULA and D. R. PAUL, *Polymer* **33** (1992) 1606.
19. H. KIM, H. KESKKULA and D. R. PAUL, *ibid.* **31** (1991) 1447.
20. L. A. UTRACKI and Z. H. SHI, *Polym. Eng. Sci.* **24** (1992) 1824.
21. U. SUNDARARAJ, C. W. MACKOSKO, R. J. ROLANDO and H. T. CHAN, *ibid.* **24** (1992) 1814.
22. G. I. TAYLOR, *Proc. R. Soc. (Lond.)* **A138** (1932) 41.
23. H. LAMB, "Hydrodynamics", 6th Edn. (Dover, New York, 1932).
24. R. J. M. BORGGREVE, R. J. GAYMANS, J. SCHUIJER and J. F. INGEN HOUSZ, *Polymer* **28** (1987) 1489.
25. E. J. MOSKALA, *J. Mater. Sci.* **27** (1992) 4883.

*Received 4 July*
*and accepted 5 July 1994*